CP Violation in the B$_s^0$ system

S. Donati

University and INFN of Pisa, Largo Pontecorvo 2, 56127 Pisa, Italy

In this paper the most recent Tevatron results concerning CP violation in the B_s system are reviewed. These are the measurement of the direct CP asymmetry in the $B_s^0 \to K^- \pi^+$ decay performed by CDF and the measurement of $\Delta\Gamma_s$ and ϕ_s performed by D0 in the $B_s^0 \to J/\psi\phi$ decay.

1. Introduction

One of the challenges for elementary particle physics is to trace all possible sources of the violation of CP symmetry. In the standard model, CP symmetry is violated through the CKM mechanism. Although the standard model picture of CP violation has so far been confirmed by all laboratory measurements, the level of CP violation in the standard model is too small to produce the observed baryon number density in the universe. One source of CP violation arises in the mixing of doublets of neutral mesons, as the K^0, composed of a down quark and a strange quark, and the B_s^0 mesons, with the down quark replaced by a bottom quark. This makes searching for CP violation in the B_s^0 decays very interesting. B hadrons are abundantly produced at the Tevatron Collider, the measured B$^+$ cross section is 2.78±0.24 μb in the region of transverse momentum $p_T(B^+) > 6.0$ GeV/c and rapidity $| \eta(B^+) |< 1$ [1]. This cross section is three orders of magnitude larger than at e^+e^- machines running at the $\Upsilon(4S)$ and the available energy allows the production of the heavier B_s^0 (and B_c and Λ_b) hadrons, although reduced by a factor $f_s/f_d(f_u)$ with respect to $B^0(B^+)$. The challenge is extracting the interesting B_s^0 signals from a level of background which is three orders of magnitude higher at production. This is achieved at CDF II and D0 with dedicated detectors, triggers and sophisticated analyses.

2. The Tevatron Collider and the CDF II and D0 Detectors

The Tevatron Collider collides 36 $p\overline{p}$ bunches at $\sqrt{s}$ = 1.96 TeV. The design instantaneous luminosity was 10^{32} cm^{-2}s^{-1} but the Tevatron now exceeds it and set the peak luminosity record at 2.8×10^{32} cm^{-2}s^{-1}. With an already integrated luminosity of 2.5 fb^{-1}, the expectation is to have integrated $\sim$8 fb^{-1} by the year 2009.

2.1. The CDF II Detector and Trigger

The elements of the CDF II detector (Fig. 1) most relevant for B physics analyses are the tracker, the
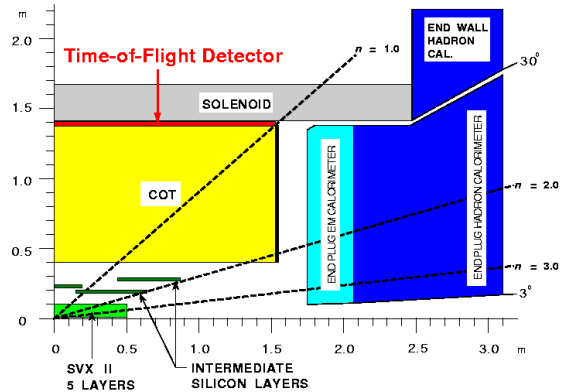

Figure 1: Quarter view of the CDF II tracker. Starting from the beamline are visible the silicon detectors (L00, SVXII and ISL), the drift chamber (COT), the Time of Flight detector and the solenoid. Also reported are the plug calorimeters. The central calorimeter and the muon chambers which surround the solenoid are not reported in this drawing.

particle identification detector and the muon system. The CDF II tracker is located within a 14.1 kG solenoidal magnetic field and it is composed of a drift chamber and of silicon detectors. There are three independent silicon detectors, SVXII, ISL and L00, for a total of eight silicon layers, 704 ladders and 722,432 channels [2], posed between the radii of 1.5 cm and of 28 cm from the beamline. The Central Outer Chamber (COT, [3]) is located outside the silicon detectors and inside the time-of-flight detector scintillators. The active volume of the COT spans 310 cm in the beam direction, 43.4 cm and 132.3 cm in radius, and the entire azimuth. The COT contains 30,240 sense wires that run the length of the chamber between two end plates. Approximately half of the wires are axial (run along the z direction) and half are small angle ($\pm2°$) stereo. The $r - \phi$ view provides information for the p_T measurement, the $r - z$ view for the η measurement. The achieved performance of the integrated CDF II tracker is a transverse momentum resolution $\sigma(p_T)/p_T^2 = 0.15$ % (GeV/c)$^{-1}$ and an impact parameter resolution $\sigma(d) = 35$ μm @2 GeV/c. This performance is crucial for the B physics analyses.

CDF II uses two complementary techniques for par-

ticle identification, one is the dE/dx measurement in the COT, the other one is the time-of-flight measurement in a dedicated detector. The COT read-out electronics allows to measure the pulse width, which is related to the amount of charge collected by the wire. The truncated mean (80 %) computed on the hits associated to a track provides a measurement of the specific ionisation (dE/dx) in the chamber. A detailed calibration of the dE/dx measurement has been performed using samples of kaons and pions from $D^{*+} \rightarrow D^0\pi^+ \rightarrow [K^-\pi^+]\pi^+$, protons from $\Lambda^0 \rightarrow p\pi^-$, and muons and electrons from $J/\psi \rightarrow \mu^+\mu^-$ and $J/\psi \rightarrow e^+e^-$. The achieved K/π separation for $p_T > 2$ GeV/c is 1.4σ. The Time-of-Flight detector (TOF, [4]) is composed of 216 scintillator bars istalled between the drift chamber and the solenoid magnet at a radius of roughly 138 cm. The time resolution on the single hit is 110 ps and the K/π separation is better than 2σ for $p_T < 1.5$ GeV/c. By combining the dE/dx and the time-of-flight measurements, the achieved K/π separation is better tha $1.4\,\sigma$ in the entire momentum range.

The CDF II central muon detector [5] is located around the outside of the central calorimeter, which is 5.5 interaction lengths thick, at a radius of 347 cm from the beam axis. The pseudorapidity coverage of the muon detector is $\mid \eta \mid< 1$.

CDF II uses a three-level system to reduce the 1.7 MHz bunch crossing rate to 100 Hz written on tape. The Level 1 is a deadtimeless 7.6 MHz synchronous pipeline with 42 cells, which allows 5.5 μs to form a trigger decision. The maximum sustainable Level 1 output rate is 30 kHz. The Level 2 is an asynchronous pipeline with an average latency of 20 μs. While the events accepted by Level 1 are being processed by Level 2 processors, they are also stored in one of the four Level 2 buffers, waiting for Level 2 trigger decision. Each buffer is emptied when the Level 2 decision for the corresponding event has been asserted: if the event has been accepted, the buffer is read out, else it is simply cleared. If the Level 2 trigger decision takes too much time and the four buffers are all filled, the Level 1 accept is inhibited. This is a source of deadtime for the CDF II trigger. The maximum Level 2 output rate is 300 Hz. The Level 3 trigger is made of a CPU farm and has a maximum output rate of 100 Hz.

The heart of the Level 1 trigger is the eXtremely Fast Tracker (XFT, [7]), the trigger track processor that identifies high transverse momentum ($p_T > 1.5$ GeV/c) charged tracks in the transverse plane of the COT. The XFT tracks are also extrapolated to the calorimeter and to the muon chambers to generate electron and muon trigger candidates.

The Online Silicon Vertex Tracker (SVT, [8]) is part of the Level 2 trigger. It receives the list of XFT tracks and the digitised pulse heights on the axial layers of the silicon vertex detector. The SVT links the XFT tracks to the silicon hits and reconstructs tracks with offline-like quality. In particular the resolution on the impact parameter, which is a crucial parameter to select B events since they tipically show secondary vertices, is 35 μm for 2 GeV/c tracks. The SVT efficiency is 85 % per track.

The Level 3 trigger is implemented on a CPU farm which allows to perform an almost offline-quality event reconstruction.

CDF II has basically three families of triggers for B physics: the dimuon trigger, the semileptonic trigger and the hadronic trigger. The dimuon trigger selects muon pairs with transverse momenum as low as 1.5 GeV/c. It is mostly used to select J/ψs and $\psi(2S)$, to reconstruct the many decay modes of the B hadrons (B^0, B^+, B^0_s, B_c, and Λ_b) containing a J/ψ decaying to muon pairs, and to select $\Upsilon \rightarrow \mu^+\mu^-$ decays, or muon pairs for the search of the rare $B \rightarrow \mu^+\mu^- X$ decays, or for $b\bar{b}$ correlation studies. The semileptonic trigger selects events with a lepton (μ or e) with $p_T > 4$ GeV/c and an SVT track with $p_T > 2$ GeV/c and impact parameter above 120 μm. The hadronic trigger selects track pairs with $p_T > 2$ GeV/c and $p_{T1} + p_{T2} > 5.5$ GeV/c, with an opening angle in the transverse plane below $135°$, impact parameter above 100 μm, a decay length above 200 μm. For the two-body decay trigger path, optimised to collect $B \rightarrow h^+h^{'-}$ decays, the track pair is requested to point back to the primary vertex, by requiring that the impact parameter of the reconstructed B is below 140 μm. To select hadronic multibody decays, like $B^0_s \rightarrow D^-_s \pi^+$, the request on the pointing back to the primary vertex has low efficiency, since the track pair provides only a partial reconstruction of the multibody decay, and it is not applied.

2.2. The D0 Detector and Trigger

The D0 detector (Fig. 2) consists of a magnetic central-tracking system, comprised of a silicon microstrip tracker and a central fiber tracker, both located within a 2 T superconducting magnet. The fiber tracker has eight thin coaxial barrels, each supporting two doublets of overlapping scintillating fibers, one doublet being parallel to the collision axis, and the other alternating by $\pm 3°$ relative to the axis. Central and forward preshower detectors located just outside of the superconducting coil in front of the calorimetry are constructed of several layers of extruded triangolar scintillator strips. The nextr layer of detection involves three liquid-argon/uranium calorimeters: a central section covering $\mid \eta \mid< 1.1$ and two endcap calorimeters that extend coverage to $\mid \eta \mid< 4.2$ all housed in separate cryostats. The muon system is located beyond the calorimetry, and consists of a layer of tracking detectors and scintillator trigger counters before 1.8 T iron toroids, followed by two similar
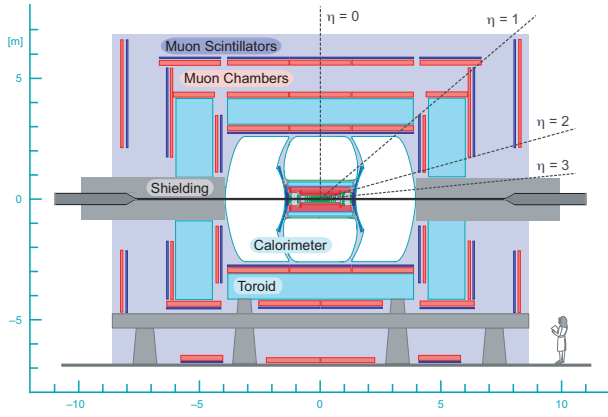
Figure 2: View of the D0 detector.

Figure 3: Invariant mass distribution of $B^0_{(s)} \to h^+h'^-$ candidates passing all selection requirements. The invariant mass is computed by assigning the pion mass to both tracks in the decay.

layers after the toroids. A muon originating in a $p\bar{p}$ collision traverses the silicon detector and the scintillating fiber tracker in the 2 T solenoidal magnetic field, the calorimeter, and the muon spectrometer and 1.8 T magnetised iron toroids. The momentum of the muon is measured twice: once by the local muon system and once by the central-tracking system. The polarities of the toroid and the solenoid magnetic fields are reversed roughly every two weeks so that the four solenoid-toroid polarity combinations are exposed to approximately the same integrated luminosity. This allows cancellation of first-order effects of the detector geometry.

The trigger and data acquisition systems are designed to accomodate the high luminosities of run II. Based on preliminary information from tacking, calorimetry, and muon systems, the output of the first level of the trigger is used to limit the rate for accepted events to 2 kHz. At the next trigger stage, with more refined information, the rate is reduced further to 1 kHz. The third and final level of the trigger, with access to all the event information, uses software algorithms and a computing farm, and reduces the output rate to 50 Hz, which is written tape. B triggers are based on single letpons ($p_T > 3.0$ GeV/c) and on muon pairs ($p_t > 2.0$ GeV/c).

3. CDF Measurement of Direct CP Asimmetry in the $B^0_s \to K^- \pi^+$ Decay

CDF II reported the first evidence of the decay and measurement of the direct CP asimmetry in the $B^0_{(s)} \to K^- \pi^+$ decay reconstructed in the data taken by the hadronic trigger (1 fb^{-1}). In the offline analysis an unbiased optimisation procedure determined a tightened selection on track-pairs fit to a common decay vertex, optimising the sensitivity for discovery and limit setting [13]. In addition to tightening the trigger cuts, the discriminating power of the B^0_s meson isola-
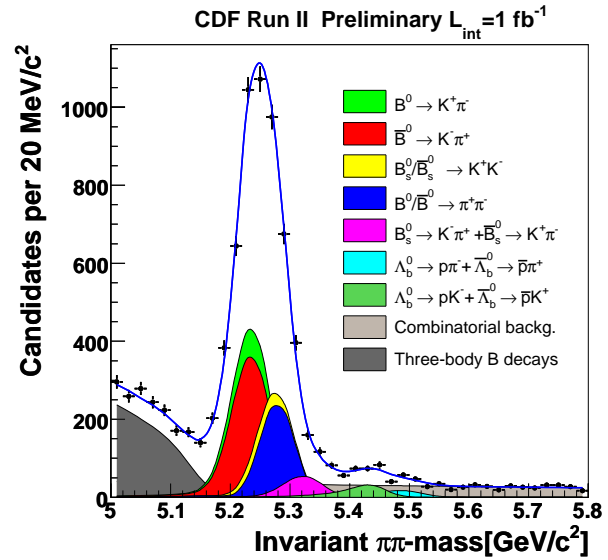
tion and of the information provided by the 3D reconstruction capability of the CDF tracking were used, allowing a great improvement in the signal purity. The resulting $\pi\pi$-mass distribution (Fig. 3) shows a clean signal of $B^0_{(s)} \to h^+h'^-$ decays. In spite of a good mass resolution (≈ 22 MeV/c^2), the various $B^0_{(s)} \to h^+h'^-$ mdoes overlap into an unresolved mass peak.

The resolution in invariant mass and in particle identification is not sufficient for separating the individual decay modes on an event by event basis, therefore an unbinned maximum likelihood fit was performed, combining kinematic and particle identification information, to statistically determine both the contribution of each mode, and the relative contributions to the CP asimmetries. For the kinematic portion, three loosely correlated variables were used to summarise the information carried by all possible values of invariant mass of the B candidate, resulting from different mass assignments to the two outgoing particles. They are: (a) the mass $M_{\pi\pi}$ calculated with the charged pion mass assignment to both particles; (b) the signed momentum imbalance $\alpha = (1 - p_1/p_2)q_1$, where $p_1(p_2)$ is the lower (higher) of the particle momenta, and q_1 is the sign of the charge of the particle momentum p_1 (Fig. 4); (c) the scalar sum of the particle momenta $p_{tot} = p_1 + p_2$. Particle identification information derives mostly from the dE/dx measurement in the drift chamber which provides a 1.4σ separation between pions and kaons in the momentum range of interest. A sample of 1.5M $D^{*+} \to D^0\pi^+ \to [K^-\pi^+]\pi^+$ decays, where the D^0
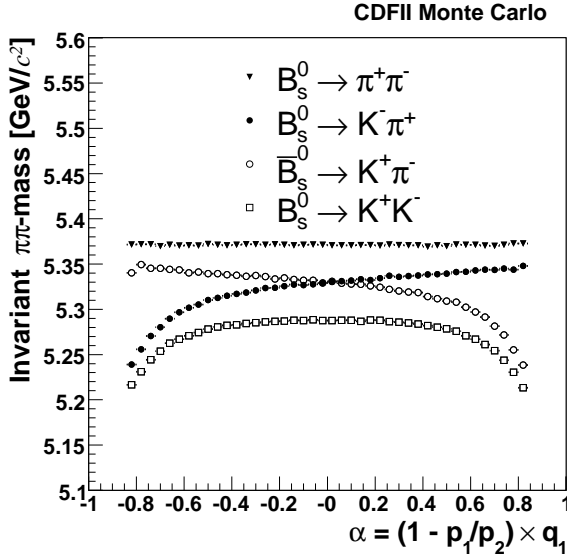 $D^{*+} \to D^0\pi^+ \to [K^-\pi^+]\pi^+$ decays, where the D^0

Figure 4: $M_{\pi\pi}$ versus signed momentum imbalance $\alpha = (1 - p_1/p_2)q_1$ for the $B_s^0 \rightarrow h^+h'^-$ decays. Similar curves are for the $B_d^0 \rightarrow h^+h'^-$ and $\Lambda_b^0 \rightarrow ph$ decays
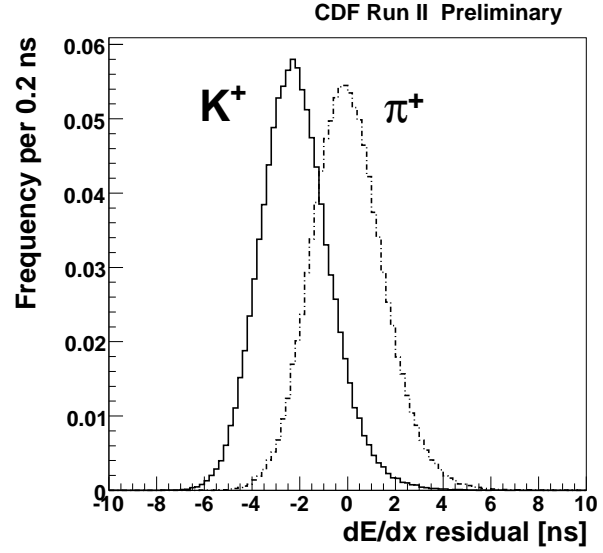

Figure 5: Tagged $D^0 \rightarrow K^-\pi^+$ decays from $D^{*+} \rightarrow D^0\pi^+ \rightarrow [K^-\pi^+]\pi^+$: distribution of dE/dx around the average pion response, for calibration samples of kaons and pions.
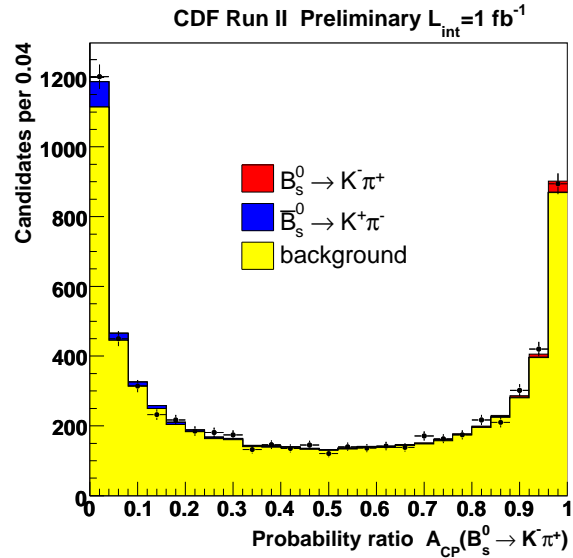

Figure 6: Likelihood ratio for the measurement of A_{CP} in the $B_s^0 \rightarrow K^-\pi^+$ decay.

decay products are identified by the charge of the D^{*+} pion, was used to calibrate the dE/dx response over the tracking volume and over time (Fig. 5). The mass resolution function was parameterised using the detailed detector simulation. To take into account non-Gaussian tails due to the emission of photons in the final state, soft photon emission was included in the simulation using recent QED calculations [14]. The quality of the mass resolution was verified using about 500k $D^0 \rightarrow K^-\pi^+$ decays and improved agreement was found between data and the simulation including the final state radiation.

In addition to the improved measurement of branching fractions of the already known modes ($B^0 \rightarrow \pi^+\pi^-$, $B^0 \rightarrow K^+\pi^-$ and $B_s^0 \rightarrow K^+K^-$) and of the direct CP asymmetry $A_{CP}(B^0 \rightarrow K^+\pi^-)$, the analysis observes three new rare modes for the first time ($B_s^0 \rightarrow K^-\pi^+$, $\Lambda_b^0 \rightarrow p\pi$ and $\Lambda_b^0 \rightarrow pK$), with a significance respectively of 8.2σ, 6.0σ and 11.5σ, which includes both statistical and systematic undertainty. To convert the yields returned from the fit into relative branching fractions, we applied corrections for efficiencies of trigger and offline selection requirements for different decay modes.

The relative efficiency corrections between modes do not exceed 20 %. Most corrections were determined from the detailed detector simulation, with some exceptions which were measured using the data. The only correction needed for the direct CP asymmetries $A_{CP}(B^0 \rightarrow K^+\pi^-)$ and $A_{CP}(B_s^0 \rightarrow K^-\pi^+)$ was a < 0.6 % shift due to the different probability for a K^+ and K^- to interact with the tracker material. The measurement of this correction has been performed

using a sample of 1M of prompt $D^0 \rightarrow K^-\pi^+$ decays reconstructed and selected using the same criteria as $B_{(s)}^0 \rightarrow h^+h'^-$ decays. Assuming the standard model expectation of $A_{CP}(D^0 \rightarrow K^-\pi^+) = 0$, the difference between the number of reconstructed $D^0 \rightarrow K^-\pi^+$ and $\overline{D}^0 \rightarrow K^+\pi^-$ provides a measurement of the detector induced asymmetry between $K^+\pi^-$ and $K^-\pi^+$. The measured branching fraction of the newly observed mode $BR(B_s^0 \rightarrow K^-\pi^+) =$

$(5.0 \pm 0.75 \pm 1.0) \times 10^{-6}$ is in agreement with the latest theoretical predictions [15], which are lower than previous predictions [16].

The analysis measures for the first time the direct CP asymmetry $A_{CP}(B_s^0 \to K^- \pi^+) = 0.39 \pm 0.15 \pm 0.08$, which favors a large CP violation in the B_s^0 decays. A robust test of the standard model can be performed by comparing the measurements of the direct CP asymmetry in the $B_s^0 \to K^- \pi^+$ and $B^0 \to K^+ \pi^-$ decays [17]. The estimated expected value for $A_{CP}(B_s^0 \to K^- \pi^+) \approx 0.37$ is in agreement with the CDF II measurement. The branching fraction $BR(B_s^0 \to K^+ K^-) = (24.4 \pm 1.4 \pm 4.6) \times 10^{-6}$ is in agreementt with the latest theoretical expectations [18]. With a large $B_s^0 \to K^+ K^-$ sample ($\approx$ 1300 ev/fb^{-1}) and the flavor taggers optimised and x_s measured, CDF has all the ingredients for a time dependent A_{CP} measurement in this mode [19], which is particularly interesting with the full statistics (8 fb^{-1}) expected for run II.

4. Measurements of $\Delta\Gamma_s$ and ϕ_s

The standard model predicts sizeable mass and decay width differences between the light and heavy eigenstates of the mixed B_s^0 system. The CP violating phase is expected to be small, thus the two mass eigenstates are expected to be CP eigenstates. Phenomena beyond the standard model may reduce the observed $\Delta\Gamma$ compared to the standard model prediction $\Delta\Gamma \approx \Delta\Gamma_{SM} \times cos(\phi_s)$ [20]. The decay $B_s^0 \to J/\psi\phi$ gives rise to both CP-even and CP-odd final states, which can be separated through a study of the time-dependent angular distribution of the decay products of the J/ψ and ϕ mesons. This allows to measure the lifetime difference between the two states and provides sensitivity to the mixing phase through the interference terms between the CP-even and CP-odd waves [21]. The angular analysis of the $B_s^0 \to J/\psi\phi$ decays has been performed both by CDF and D0. Both experiments reconstruct the decay modes in samples collected by the muon triggers, which require the presence of muon segments in the muon detectors matched to central tracks. In the offline analysis J/ψ and ϕ candidates are required to be consistent with coming from a common vertex and to have an invariant mass compatible with the B^0 mass The proper decay length ct is defined by the relation $ct = L_{xy}^B \cdot M_{B_s^0}/p_T$, where $M_{B_s^0}$ is the measured mass of the B_s^0 candidate. A simultaneous unbinned maximum likelihood fit is performed to the mass, proper decay length and three decay angles. In the coordinate system of the J/ψ rest frame, where the ϕ meson moves in the x direction, the z axis is perpendicular to the decay plane of $\phi \to K^+ K^-$ and $p_y(K^+) > 0$, the transversity polar and azimuthal angles (θ, ϕ) describe the direction of
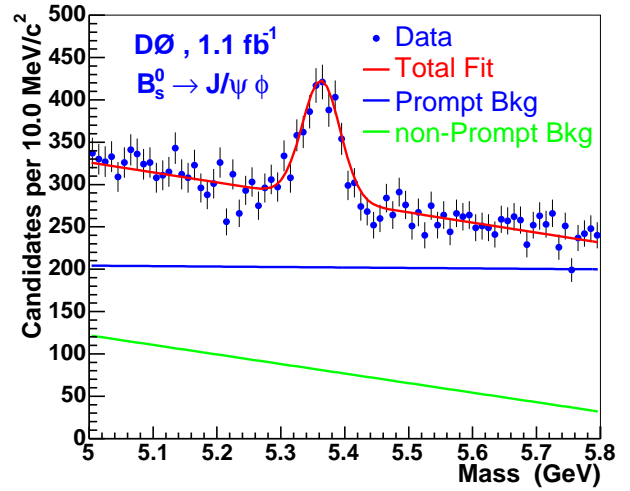

Figure 7: Invariant mass distribution of the $(J/\psi, \phi)$ system for the B_s^0 candidates. The curves are projections of the maximum likelihood fit.

the μ^+, and ψ between $\vec{p}(K^+)$ and $-\vec{p}(J/\psi)$ in the ϕ rest frame. From the analysis of 1.1 fb^{-1} of data D0 estimates a yield of 1039 ± 45 B_s^0 events, with an average lifetime $\tau(B_s^0) = 1.52 \pm 0.08(stat) \pm 0.03(syst)$ ps and a width difference between the two mass eigenstates $\Delta\Gamma = 0.12^{+0.08}_{-0.10}(stat) \pm 0.02(syst)$ ps^{-1}. Allowing for CP violation in the B_s^0 mixing the first direct constraint on the CP violating phase $\phi_s = -0.79 \pm 0.56(stat) \pm 0.14(syst)$ is obtained [22]. Using a sample of 355 pb^{-1} of data CDF reconstructed 203 ± 15 B_s^0 decays and with an angular analysis measured $\tau(B_s^0) = 1.40^{+0.15}_{-0.13}(stat) \pm 0.02(syst)$ ps and $\Delta\Gamma = 0.47^{+0.19}_{-0.24}(stat) \pm 0.01(syst)$ ps^{-1} [23]. CDF is currently updating the analysis to 1 fb^{-1} of data. At the moment of writing these proceedings the CDF results are not public yet.

4.1. D0 charge asymmetry measurement

D0 has measured the dimuon charge asymmetry $A = (N^{++} - N^{--})/(N^{++} + N^{--})$, where N^{++} (N^{--}) is the number of events with two positive (negative) muon candidates passing selection cuts. This inclusive, tagged measurement is sensitive to CP violation in B_s^0 mixing. The dimuon charge asymmetry A has contributions from both B^0 and B_s^0, therefore this measurement at the Tevatron collider is complementary to similar measurements at B factories that are sensitive only to A_{B^0}, not $A_{B_s^0}$. The D0 measurement is $A = -0.0092 \pm 0.0044(stat) \pm 0.0032(syst)$ [24]. There are several sources of systematic errors contributing to this measurement, such as the detector effects, which are significantly reduced by averaging over the samples collected with the different combinations of magnetic field polarities, the different $K^\pm$ interaction rates with the detector material which
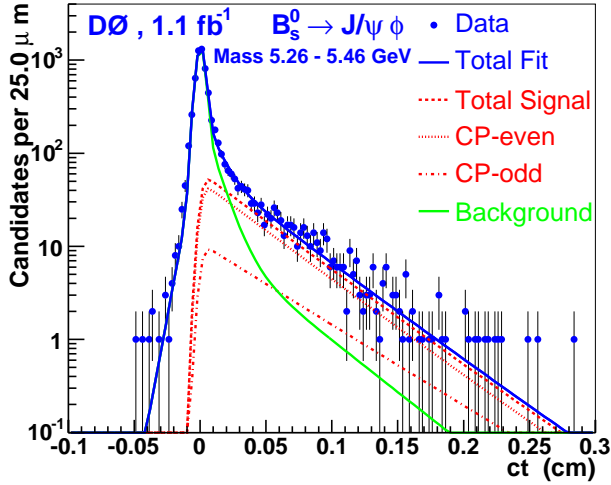
Figure 8: Proper decay length ct of the $B_s^0 \to J/\psi\phi$ candidates in the signal mass region. The curves show the signal contribution, the CP-even and CP-odd contributions of the signal, the background and the total curve.
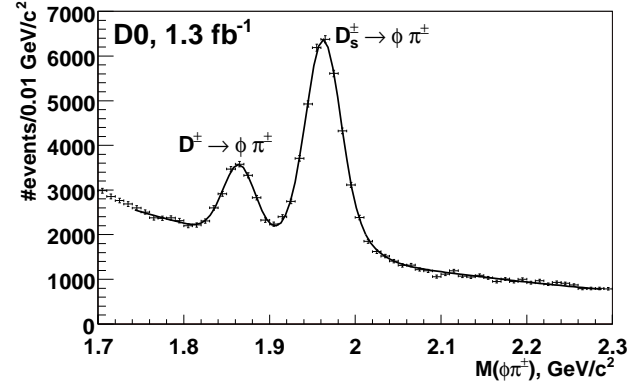

Figure 9: Invariant mass distribution $M(\phi\pi)$ for the selected B_s^0 candidates. The curve shows the result of a fit with a double gaussian function for the D signals and an exponential for the background.

generates different $K^\pm \to \mu^\pm$ rates, the presence of the dimuon cosmic rays, and the hadronic punch-through. Both B_d^0 and B_s^0 contribute to this quantity ($A = A_d + \alpha \cdot A_s$, where A_d and A_s are respectively the charge asymmetries of the B^0 and B_s^0 semileptonic decays, and α is a coefficient which depends on the B^0 and B_s^0 production rates and mixing parameters, which can be computed using the world average values $\alpha = 0.70 \pm 0.07(syst) \pm 0.10(PDG)$). The asymmetry A_d has been measured at B factories where only B^0 and $B^\pm$ are produced, and the resulting average value is $A_d = -0.0047 \pm 0.0046$ [25]. This measurement can be used to extract A_s from the measurement of A and the resulting value is $A_s = -0.0064 \pm 0.0101$, where the statistical and systematic uncertainties are added in quadrature.

D0 has also measured a time integrated flavour untagged charge asymmetry A_s^{unt} in the semileptonic B_s^0 decays, defined as $A_s^{unt} = [N(\mu^+ D_s^-) - N(\mu^- D_s^+)]/[N(\mu^+ D_s^-) + N(\mu^- D_s^+)]$ where the $\mu^\pm D_s^\mp$ pairs are produced in the semileptonic B_s^0 decays. This asymmetry is called untagged since the initial flavor of the B_s^0 meson is not determined. The measurement has been performed in a dataset of about 1.3 fb^{-1} of integrated luminosity, using the decay $B_s^0 \to \mu D_s \nu X$, with $D_s \to \phi\pi$, $\phi \to K^- K^+$. B_s^0 candidates were reconstructed by clustering a muon with $p_T > 2.0$ GeV/c with three charged tracks, two of which assigned the kaon mass and required to have an invariant mass (1.004 GeV/c^2 < $M(K^+K^-)$ < 1.034 GeV/c^2) consistent with that of a ϕ meson. The optimal selection on several discriminating variables (the angle between the D_s and the K momenta in

the K^+K^- center of mass frame, the isolation of the (μD_s) system, the χ^2 of the D_s vertex, the invari-

ant masses $M(\mu D_s)$ and $M(K^+K^-)$ and $p_T(K^+K^-)$) was determined by maximising the predicted ratio $S/\sqrt{S+B}$. The resulting mass distribution of the $D_s^\pm$ candidates is reported in Fig. 9. The measured value of the time integrated untagged charge asymmetry is $A_s^{unt} = [1.23 \pm 0.97(stat) \pm 0.17(syst)] \times 10^{-2}$. The main systematics (added in quadrature in the final result) are due to the different $\pi^\pm$ interaction with the material, the estimate of the B_s^0 fraction in the μD_s sample and the fitting procedure (estimated by varying the masses and widths of the peaks and the slope of the background by 1σ). Statistics dominates the error on this measurement and it will be improved in the future with the increase of statistics and addition of new decay modes [27].

The two above D0 measurements are nearly independent as well as the systematic uncertainties. Thus they can be combined to give the best estimate of the charge asymmetry in the semileptonic B_s^0 decays $A_s = 0.0001 \pm 0.0090$. A_s can be related to the CP phase ϕ_s by the formula $A_s = (\Delta\Gamma_s/\Delta M_s) \cdot tan(\phi_s)$ [28]. Using the CDF II measurement $\Delta M_s = 17.8 \pm 0.1$ ps^{-1} [29] the following constraint is obtained $\Delta\Gamma_s \cdot tan(\phi_s) = A_s \cdot \Delta M_s = 0.02 \pm 0.16$ ps^{-1}. The fit to the $B_s^0 \to J/\psi\phi$ data has been repeated by D0 including the above constraint from the measuremnt of A_s and the likelihood contours are presented in Fig. 10 and Fig. 11,respectively in the $\Delta\Gamma_s$-τ_s plane and $\Delta\Gamma_s$-ϕ_s plane. There is an unresolved 4-fold ambiguity of the solutions. For the solution with $\phi_s < 0$ and smaller absolute value, the decay width and CP violating phase are measured to be $\Delta\Gamma_s = 0.13 \pm 0.09$ ps^{-1} and $\phi_s = -0.70^{+0.47}_{-0.39}$, consistent with the standard model predictions. The measurement uncertainty is dominated by the limited statistics.
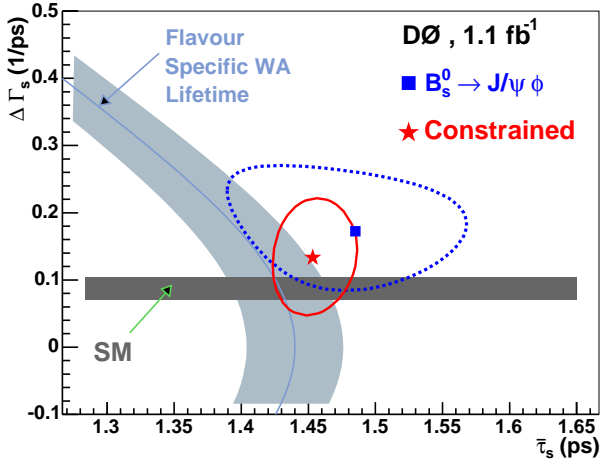
Figure 10: Error ellipse in the $\Delta\Gamma_s$ versus τ_s plane for the fit to the $B_s^0 \to J/\psi\phi$ data and for the fit with the constraint from the two D0 measurements of the charge asymmetry in the semileptonic B_s^0 decay, and from the world average flavor specific lifetime. Also shown is the 1σ band representing the world average result for τ_{fs} and the 1σ band representing the theoretical prediction $\Delta\Gamma_s = 0.088 \pm 0.017$ ps^{-1} [26]
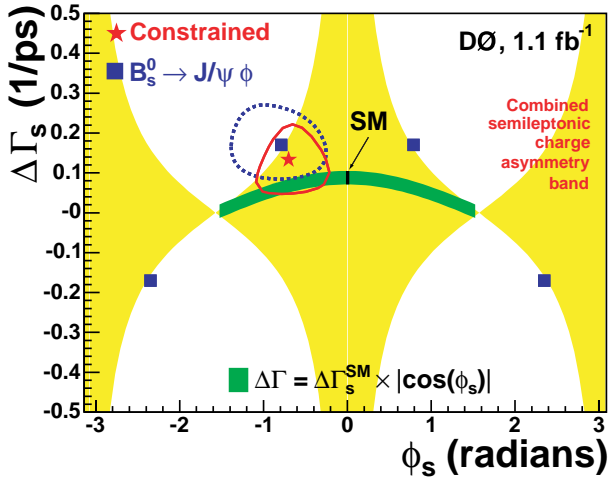

Figure 11: Error ellipse in the $\Delta\Gamma_s$ versus ϕ_s plane for the fit to the $B_s^0 \to J/\psi\phi$ data and for the fit with the constraint from the two D0 measurements of the charge asymmetry in semileptonic B_s^0 decay and from teh world average flavor-specific lifetime. The central values for all four solutions of the unconstrained fit are indicated by blue squares. Also shown is the band representing the relation $\Delta\Gamma_s = \Delta\Gamma_s^{SM} \times |cos(\phi_s)|$ with $\Delta\Gamma_s^{SM} = 0.088 \pm 0.017$ ps^{-1}.

5. Conclusions

In this paper we have reviewed CDF and D0 results concerning CP violation in the B_s^0 sector. Both collaborations have been very active in this area. CDF has performed a measurement of the direct CP asymmetry in the $B_s^0 \to K^-\pi^+$ decay mode using the

data collected by the hadronic trigger. Both collaborations have performed angular analyses of the $B_s^0 \to J/\psi\phi$ which provide measurements of $\Delta\Gamma_s$ and ϕ_s. D0 has performed charge asymmetry measurements in the single muon and dimuon samples. With the 2.5 fb^{-1} already on tape and the 8 fb^{-1} expected by 2009 the CDF and D0 collaborations are confident to have many more and better results soon.

References

[1] A. Abulencia et al., the CDF Collaboration, Phys. Rev. D **75**, 012010 (2007).
[2] A. Sill et al., Nucl. Instrum. Meth. A530:1 (2004).
[3] T. Affolder et al., Nucl. Instrum. Meth. A526:249 (2004).
[4] D. Acosta et al., Nucl. Instrum. Meth. A518:605 (2004).
[5] G. Ascoli et al., Nucl. Instrum. Meth. A268:33 (1988).
[6] L. Balka et al., Nucl. Instrum. Meth. A267:272 (1988). M. Alborw. et al., Nucl. Instrum. Meth. A453:84 (2000).
[7] E. J. Thomson et al., IEEE Trans. on Nucl. Sc. vol. 49, n. 3 (2002).
[8] A. Bardi et al., Nucl. Instrum. Meth. A485:178 (2002).
[9] E. J. Thomson *et al.*, IEEE Trans. Nucl. Sci. 49, 1063 (2002)
[10] W. Ashmanskas *et al.*, Nucl. Instrum. Meth. A518: 532, (2004)
[11] D. Acosta et al., Phys. Rev. D71, 032001 (2005).
[12] E. J. Thomson et al., IEEE Trans. Nucl. Sci. 49, 1063 (2002).
[13] G.Punzi eConf **C030908**, MODT002 (2003): arXiv:physics/0308063.
[14] E. Baracchini and G. Isidori, Phys. Lett. **B633** (2006) 309.
[15] A.R. Williamson, J. Zupan, Phys. Rev. **D74** (2006) 014003.
[16] Xian-qiao Yu et al., Phys. Rev. **D71** (2005) 074026.
[17] H. J. Lipkin, Phys. Lett. **B621** (2005) 126, M. Gronau, Phys. Lett. B **492** (2000) 297.
[18] S. Descotes-Genon et al., Phys. Rev. Lett **97** (2006) 061801.
[19] R. Fleischer,"$B_{s,d} \to \pi\pi, \pi K, KK$: Stauts and Prospects" arXiv:0705.1121.
[20] I. Dunietz et al, Phys. Rev. **D63** (2001) 114015.
[21] A. S. Dighe, I. Dunietz and R. Fleischer, Eur. Phys. J. C **6** (1999) 647.
[22] V. M. Abazov et al, Phys. Rev. Lett. **98** (2007) 121801.
[23] D. Acosta et al., Phys. Rev. Lett. **94** (2005) 101803.

[24] V. M. Abazov et al., Phys. Rev. **D74** (2006) 092001.

[25] E. Barberio et al., "Averages of b-hadron properties at the end of 2006", arXiv:0704.3575.

[26] A. Lenz, and U. Nierste, hep-ph/0612167, M. Beneke et al., Phys. Lett. B **576** (2003) 173,

M. Beneke et al., Phys. Lett. B **459** (1009) 631.

[27] V. M. Abazov et al., Phys. Rev. Lett. **98** (2007) 151801.

[28] M. Beneke et al., Phys. Lett. B **576** (2003) 173.

[29] A. Abulencia et al., Phys. Rev. Lett. **97** (2006) 242003.